International Journal of Heat and Fluid Flow 30 (2009) 1044–1053

Contents lists available at ScienceDirect

International Journal of Heat and Fluid Flow

journal homepage: www.elsevier.com/locate/ijhff

Leray-α simulations of wall-bounded turbulent flows

Maarten van Reeuwijk [a,*], Harm J.J. Jonker [b], Kemo Hanjalić [b,c]

[a] Department of Civil and Environmental Engineering, Imperial College London, Imperial College Road, London SW7 2AZ, United Kingdom
[b] Department of Multi-Scale Physics and J.M. Burgers Center for Fluid Dynamics, Delft University of Technology, Lorentzweg 1, 2628 CJ Delft, The Netherlands
[c] Department of Mechanics and Aeronautics, University of Rome, "La Sapienza", Rome, Italy

ARTICLE INFO

Article history:
Received 3 April 2009
Received in revised form 5 August 2009
Accepted 5 August 2009
Available online 5 September 2009

Keywords:
LES
Leray-α
Regularization model
Turbulence
Wall-bounded flow
Buoyancy driven flow

ABSTRACT

The Leray-α model reduces the range of active scales of the Navier–Stokes equations by smoothing the advective transport. Here we assess the potential of the Leray-α model in its standard formulation to simulate wall-bounded flows. Three flow cases are considered: plane channel flow at $Re_\tau = 590$, Rayleigh–Bénard convection at $Ra = 10^7$ and $Pr = 1$, and a side-heated vertical channel at $Ra = 5 \times 10^6$ and $Pr = 0.7$. The simulations are compared to results from a well resolved and coarse DNS. It is found that for all three flow cases, the variance in the velocity field increases as the filter width parameter a is increased, where a is connected to the filter width as $\alpha_i = a\Delta x_i$, with Δx_i the local grid size. Furthermore, the viscous and diffusive wall regions tend to thicken relative to the coarse DNS results as a function of a. In the cases where coarse DNS overpredicts wall gradients (as for Rayleigh–Bénard convection and the side-heated vertical channel), the thickening is beneficial. However, for the plane channel flow, coarse DNS underpredicts the wall-shear velocity, and increasing a only degrades the results. It is shown that buoyancy effects need to be included with care, because of the close relation of turbulent heat flux and the production of turbulent kinetic energy.

1. Introduction

The usual way to surmount the computational complexity of high Reynolds number turbulent flows and the exorbitant grid resolution demands of high Reynolds number turbulent flows is to average or filter the Navier–Stokes equations. With such pre-processing of the equations, one ends up with unclosed stresses which need to be modeled. In large-eddy simulations, the unclosed stresses are usually modeled with eddy-diffusivity type models. An alternative way of modeling is to smooth the dynamics of the Navier–Stokes equations by a direct modification of the advective terms (Holm, 1999; Foias et al., 2001; Cheskidov et al., 2005; Geurts and Holm, 2006). This allows one to derive the corresponding subscale model without any further assumptions, provided the employed filter $\mathscr{L}$ is invertible. The modification can be chosen such that important physical properties of the Navier–Stokes equations are preserved, such as energy, helicity, the Kelvin circulation theorem, or symmetries.

The Leray-α model (Cheskidov et al., 2005; Geurts and Holm, 2006; van Reeuwijk et al., 2007) is the simplest regularization model. For this model, the advective operator $\partial_j u_j u_i$ is replaced by $\partial_j \widetilde{u}_j u_i$, where the filtered velocity $\widetilde{u}_i = \mathscr{L}(u_i)$ and $\mathscr{L}$ is a filter operation. Historically, this model was used to prove existence and regularity of u_i, as well as convergence to the Navier–Stokes solution as the filter width tends to zero (Leray, 1934). Analytical estimates invoking Prandtl–Blasius arguments (Cheskidov et al., 2005) predict an excellent match for the laminar, transitional and turbulent regime, although the physical relevance of the solutions in the turbulent regime with respect to the boundary conditions and turbulence intensities may be questioned (van Reeuwijk, 2007, Appendix C). The Leray-α model has been used for the simulation of the turbulent mixing layer, and showed superior accuracy in comparison with dynamic eddy-viscosity models, in particular with respect to the quality of the small resolved scales (Geurts and Holm, 2006). The explicit filtering concept in LES can be traced back to Clark et al. (1979), although that model was originally proposed by Leonard (1974).

The Lagrangian averaged Navier–Stokes-α (LANS-α) model (Holm et al., 1998, 2002; Chen et al., 1999a,b,c; Holm, 1999; Foias et al., 2001; Mohseni et al., 2003; Marsden and Shkoller, 2003) in addition, possesses a filtered Kelvin circulation theorem. The LANS-α model has been successful in simulations of homogeneous isotropic turbulence (Chen et al., 1999c; Mohseni et al., 2003) and for the temporal mixing layer (Geurts and Holm, 2006). A regularization approach which preserves the skew-symmetry of the advective operator has been recently proposed by Verstappen (2008). Here, the energy, enstrophy (in 2D) and helicity are conserved, and accurate results are obtained with coarse simulations of plane channel flow.

* Corresponding author.
E-mail address: m.vanreeuwijk@imperial.ac.uk (M. van Reeuwijk).

0142-727X/$ - see front matter Crown Copyright © 2009 Published by Elsevier Inc. All rights reserved.
doi:10.1016/j.ijheatfluidflow.2009.08.001

Given the excellent results obtained with the Leray-α model the turbulent mixing layer (Geurts and Holm, 2006), it is a natural step to assess whether the Leray-α model performs as well for wall-bounded flows. In this paper, we study three canonical flow cases which represent a wide range of problems occurring in practical situations. The first is a plane channel flow, which is one of the standard test cases for turbulence models. The main production mechanism of turbulent kinetic energy for this flow is by shear production. The second test case is Rayleigh–Bénard convection, for which the turbulence is created purely by buoyancy production. This is a challenging test case because of the sensitive dependence of the heat-transfer on the turbulent dynamics. The third test case is a side-heated vertical channel, for which turbulent kinetic energy is produced both by shear and buoyancy. This test-case is challenging because it exhibits counter-gradient turbulence heat and momentum fluxes (Hanjalić, 2002).

In this study, we perform a coarse DNS simulation for each flow case. The resolution for this simulation is chosen such that the turbulence statistics have degraded relative to the resolved DNS solution, but the numerical solution is not dominated by wiggles. This simulation is then taken as the reference. The expectation is that the Leray-α model will improve on these results by modifying the advective transport. The filter used to smooth the transport velocity is associated with the Helmholtz operator, as proposed in the original formulation of the Leray-α model (Cheskidov et al., 2005). In order to avoid excessive smoothing in the viscous and diffusive wall regions, a non-uniform filter width is used in the wall-normal direction, which is related to the local grid size. The non-uniform filtering gives rise to a non-solenoidal filtered velocity field. As shown in (van Reeuwijk et al., 2007), a non-solenoidal velocity field can result in spurious production of TKE very close to the wall, which degrades the performance of the Leray-α model. In order to circumvent this issue, a projection method is used to ensure that the filtered velocity be solenoidal.

The details of the Leray-α model are outlined in Section 2. A preliminary study (van Reeuwijk et al., 2007) showed that for Rayleigh–Bénard convection, filtering with a constant filter size leads to an artificial thickening of the hydrodynamic and thermal boundary layer and significantly increased variances. As properly resolving viscous and diffusive wall region is of primary importance for wall-bounded flows, a space-varying filter size is applied in the wall-normal direction which scales with the grid resolution. This has implications for the velocity field, and the details about enforcing a divergence-free smoothed velocity field $\widetilde{u}_i$ when using a space-varying filter (van Reeuwijk et al., 2006) are discussed in Section 3. The simulations for the channel flow, Rayleigh–Bénard convection and the side-heated convection are discussed in Section 4. The simulation of buoyancy-driven flows requires an extension of the momentum equation with the buoyancy force and an additional temperature equation. It turns out for the adopted formulation, the direct coupling between the turbulent heat-flux and the buoyancy production of turbulent kinetic energy is lost, which is particularly problematic for Rayleigh–Bénard convection (Section 5 and Appendix A). Several suggestions are presented to correct for this undesired side effect. Concluding remarks are made in Section 6.

2. Leray-α regularization

The governing equations for the Leray-α model are

$$\partial_t u_i + \widetilde{u}_j \partial_j u_i = \nu \partial_j^2 u_i - \partial_i p + f_i, \tag{1}$$

$$\partial_i u_i = 0, \tag{2}$$

$$(1 - \partial_j \alpha_j^2 \partial_j)\widetilde{u}_i = u_i, \tag{3}$$

with u_i the velocity, p the pressure, ν the kinematic viscosity and f_i a body force. As can be seen in (1), the regularization modeling approach results in a mixed formulation of filtered and unfiltered quantities. Even though u_i is unfiltered it should not be considered a velocity coming from direct numerical simulation (DNS) because of the modified nonlinearity in (1). Therefore, both u_i and $\widetilde{u}_i$ are regularized variables. The variable α_i corresponds to the filter width which can have different values per direction and varies in the wall-normal direction. The filter $\mathscr{L}$ is given by the inverse of the elliptic equation (3) and boundary conditions; we will denote the filtering operation as

$$\widetilde{u}_i = \mathscr{L}(u_i) = (1 - \partial_j \alpha_j^2 \partial_j)^{-1}\, u_i. \tag{4}$$

This is the standard filter used for analytical studies of the Leray-α and LANS-α model (Foias et al., 2001; Cheskidov et al., 2005). Naturally, other filters could be used as well, as the effect of the filtering would (hopefully) be restricted to the small scales only. One advantage of using a formulation like (3) is in the natural treatment of boundaries. However, solving (3) is quite costly, and care should be taken to ensure the incompressibility of the filtered velocity $\widetilde{u}$ (van Reeuwijk et al., 2006).

The Leray-α model does not add additional dissipation to the equations. Indeed, the equation can be written in an LES template as

$$\partial_t u_i + \partial_j u_j u_i + \partial_i p - \nu \partial_j^2 u_i = \partial_j m_{ij}, \tag{5}$$

where m_{ij} is the subfilter model, which is given by $m_{ij} = u_j'' u_i$. Here, $u_j'' = u_j - \widetilde{u}_j$ is the high wavenumber part of u_i. Multiplying m_{ij} with u_i results in $u_i \partial_j m_{ij} = \partial_j\left(u_j'' \frac{1}{2} u_i^2\right)$, which shows that energy is only redistributed and not dissipated.

One can also derive the implied subfilter scale model of the Leray-α model in terms of the filtered velocity $\widetilde{u}$. Filtering (1) with $\mathscr{L}$ leads to an explicitly filtered LES template, given by

$$\partial_t \widetilde{u}_i + \partial_j \widetilde{u}_j \widetilde{u}_i + \partial_i \widetilde{p} - \nu \partial_j^2 \widetilde{u}_i = \partial_j \widetilde{m}_{ij}, \tag{6}$$

but with a non-standard asymmetric subfilter term

$$\widetilde{m}_{ij} = \widetilde{u}_j \widetilde{u}_i - \widetilde{\widetilde{u}_j u_i} = \widetilde{u}_j \widetilde{u}_i - \widetilde{u}_j \widetilde{u}_i + \widetilde{u_j'' u_i}. \tag{7}$$

The Leray-α model reduces the number of active scales by slowing down the energy cascade at small scales. This is shown schematically in Fig. 1 for the energy spectrum E of unfiltered velocity. The wavenumber associated with the filter size is k_α. For $k < k_\alpha$, the energy cascade is unaffected which results in the classical $E \propto k^{-5/3}$ spectrum. However, for $k > k_\alpha$, the filter affects the cascade timescale and the spectrum is modified to $E \propto k^{-1/3}$. Because of the higher variances at small scales, the dissipation will take place on larger scales than the Kolmogorov scale with associated wave number k_η. Note that the energy density spectrum of the filtered velocity

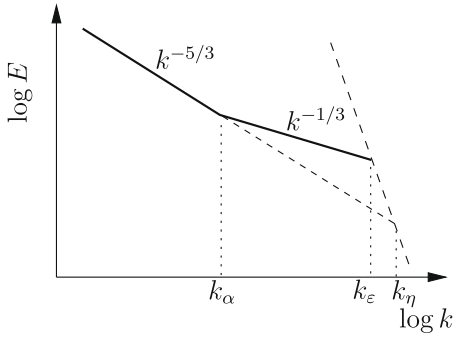

Fig. 1. Sketch of a typical spectrum for the unfiltered velocity u_i of the Leray-α model.

$\widetilde{E} = \widehat{\mathscr{L}}^2(k)E(k)$ falls off steeply as $\widetilde{E} \propto k^{-13/3}$ beyond k_α (see also Cheskidov et al., 2005).

3. Enforcing a nondivergent $\widetilde{u}_i$ field

Enforcing the incompressibility condition $\partial_j u_j = 0$ does not automatically ensure that $\partial_j \widetilde{u}_j = 0$ for a wall-bounded flow. For uniform α, the solution $f(\mathbf{x}) = \partial_i \widetilde{u}_i$ of the homogeneous differential equation $f - \partial_j \alpha_j^2 \partial_j f = 0$ is nontrivial and does not vanish upon applying the boundary conditions (van Reeuwijk et al., 2006). The main problem with $\partial_j \widetilde{u}_j \neq 0$ is that the purely redistributive character of advection is lost, which can be demonstrated by considering the effect on the balance of the turbulent kinetic energy (TKE). The turbulent transport of TKE by fluctuations can be calculated by taking the advection term $\partial_j(\widetilde{u}_j' u_i')$ from the equation of velocity fluctuations, multiplying it by u_i' and averaging:

$$\overline{u_i' \partial_j (\widetilde{u}_j' u_i')} = \partial_j \overline{\widetilde{u}_j' e'} + \overline{e' \partial_j \widetilde{u}_j'}, \tag{8}$$

with $e' = \frac{1}{2} u_i' u_i'$. The first term on the right-hand side is in divergence-form and hence purely redistributive. The second term is a production/destruction term, which normally vanishes because the fluctuating field is divergence free. However, when $\partial_j \widetilde{u}_j \neq 0$ this term can become nonzero, thereby allowing for spurious TKE production and destruction. As was shown for Rayleigh–Bénard convection at $\mathrm{Ra} = 10^5$ and $\mathrm{Pr} = 1$, the term $\overline{e' \partial_j \widetilde{u}_j'}$ is responsible for significant energy production in the hydrodynamic boundary layer (up to 25% of the volume-averaged production) (van Reeuwijk et al., 2006).

A nonuniform filter width α, creates another opportunity for $\partial_j \widetilde{u}_j \neq 0$. Applying the filter $\mathscr{L}$ to the divergence of the unfiltered velocity gives that $\mathscr{L}(\partial_j u_j) = \partial_j \mathscr{L}(u_j) + [\mathscr{L}, \partial_j] u_j$, where the brackets represent the commutator defined as $[A, B] \equiv AB - BA$. Therefore, the divergence of the filtered velocity is given by

$$\partial_j \widetilde{u}_j = [\partial_j, \mathscr{L}] u_j + \mathscr{L}(0). \tag{9}$$

This shows both ways in which $\widetilde{u}$ can cease to be divergence-free. First the commutator may not vanish because of a nonuniform filter width $\alpha(\mathbf{x})$. Second, the term $\mathscr{L}(0)$ is nonzero when the solution $f(\mathbf{x}) = \partial_i \widetilde{u}_i$ of the homogeneous differential equation $f - \partial_j \alpha_j^2 \partial_j f = 0$ does not yield $f = 0$ after applying the boundary conditions, as discussed above. In van Reeuwijk et al. (2006), several methods were proposed to maintain a nondivergent $\widetilde{u}_i$ field: enforcing $\partial_j \widetilde{u}_j = 0$ directly (and thus dropping $\partial_j u_j = 0$), letting α vanish at the wall, using free-slip boundary conditions for $\widetilde{u}_i$ and introducing a projection method. Of these four options, only the projection method can be successfully applied for nonuniform filters $\alpha(\mathbf{x})$, so this is a convenient choice. The projection method (e.g. Ferziger and Perić, 2002) adds a gradient $\partial_i \phi$ to (4) as $\widetilde{u}_i + \partial_i \phi = \mathscr{L}(u_i)$ and solves a Poisson equation $\partial_j^2 \phi = \partial_i \mathscr{L}(u_i)$ to make $\widetilde{u}_i$ incompressible. The boundary conditions imposed on $\widetilde{u}_i$ and ϕ are equivalent to the conditions imposed on u_i and p; $\widetilde{u}_i = 0$ and $\partial_n \phi = 0$, respectively.

With the projection included, the filtered velocity $\widetilde{u}_i$ is related to the unfiltered velocity u_i by a filter $\mathscr{G}$ as

$$\widetilde{u}_i = \mathscr{G}(\mathbf{u}) = P_{ij} \circ \mathscr{L}(u_j), \tag{10}$$

where P_{ij} is the projection operator. Note that $\mathscr{G}$ takes the complete velocity vector as its argument, as opposed to $\mathscr{L}$ which only requires one velocity component at a time.

The grid resolution is normally a good indication for the location of the most demanding flow features. Therefore, we couple the filter size α_i directly to the grid resolution by a parameter a as

$$\alpha_i = a \Delta x_i. \tag{11}$$

Note that the filter size is anisotropic. In the wall-normal direction, the grid is clustered towards to wall so that the filter is small near the wall and larger in the midplane. The smoothing parameter a is varied between $0 < a < 1$, for which the typical filter width spans up to four grid cells. This can be shown by calculating the filter width Δ from (e.g. Geurts and Holm, 2006):

$$\frac{1}{\Delta} = \int_{-\infty}^{\infty} G_\alpha^2(x, x') dx', \tag{12}$$

where G_α is a normalized filter kernel. The free-space Green's function associated with the Helmholtz equation is

$$G_\alpha(x, x') = \frac{1}{2\alpha} \exp\left(-\frac{|x - x'|}{\alpha} \right). \tag{13}$$

Substitution of the above expression and (11) into (12) leads to $\Delta = 4a\Delta x_i$.

The projection method has been implemented in our code for direct simulation as a two-step process. In the first step, the elliptic equation (3) is solved by a direct method which takes advantage of the homogeneous directions. In the second step, the projection method is used to make this field divergence free. The code is based on staggered finite differences and uses second order central differences in space and a second order Adams–Bashforth scheme in time (van Reeuwijk, 2007). The code is fully parallellized and supports grid clustering in wall-normal direction. Special care has been taken to preserve the purely redistributive character of the advection scheme on the nonuniform grid by using a symmetry-preserving discretization (Verstappen and Veldman, 2003).

4. Results

4.1. Plane channel flow

The first wall-bounded flow case under consideration is plane channel flow. Here we compare results for the Leray-α model with direct simulations (Moser et al., 1999) at $\mathrm{Re}_\tau = 590$. The coordinate system is defined in Fig. 2a, with the x-, y- and z-coordinate aligned with the streamwise, wall-normal and spanwise direction, respectively. The medium is air with a kinematic viscosity $\nu = 10^{-5}$ m^2/s and the domain size $L_x \times L_y \times L_z$ is $2\pi\delta \times 2\delta \times \pi\delta$, where $\delta = 1$ m is the channel halfwidth. No-slip boundary conditions are applied to the top and bottom plates, and periodic boundary conditions are used on the sidewalls. The average velocity is fixed at $U = 0.115$ m/s for all simulations. At full DNS resolution $(384 \times 384 \times 256)$ cells, this flowrate results in a shear-Reynolds number $\mathrm{Re}_\tau = 610$. For the Leray-α and coarse DNS simulations, the grid has been chosen such that the grid is too coarse for a good solution without a subgrid model, but fine enough so that the solution is not dominated by wiggles. For the plane channel flow this resulted in a grid of $64 \times 64 \times 32$ cells with strong grid clustering (up to 16% near the walls). All results were averaged for about 60 typical turnovers (based on a typical turnover time $t^* = U/(2\delta)$).

Three different values of the filter parameter a are used here: $a = 0.25$, 0.50 and 1.00. As discussed before, the filter is proportional to the local grid resolution as $\alpha_i = a\Delta x_i$, and due to the grid clustering in the wall-normal direction, the filter is much smaller near the wall than in the midplane (Fig. 3). In this way, the artificial thickening of the viscous wall region (viscous sublayer and buffer layer (Pope, 2000)). due to the filtering which hampered preliminary simulations (van Reeuwijk et al., 2007) is minimized.

Shown in Fig. 2b, are the average velocity profiles in plus-units, defined as $\overline{u}^+ = \overline{u}/u_\tau$ and $y^+ = y u_\tau/\nu$. Here u_τ is the friction velocity defined as $u_\tau = \sqrt{\tau_w/\rho}$, where $\tau_w = \mu \partial_y \overline{u}|_w$ is the shear stress at the wall. As can be expected, the coarse DNS velocity profile lies above the reference profile, which reflects an underestimated wall-shear stress. The results for the Leray-α model are denoted by the circles, squares and crosses for $a = 0.25$, 0.50 and 1.00,

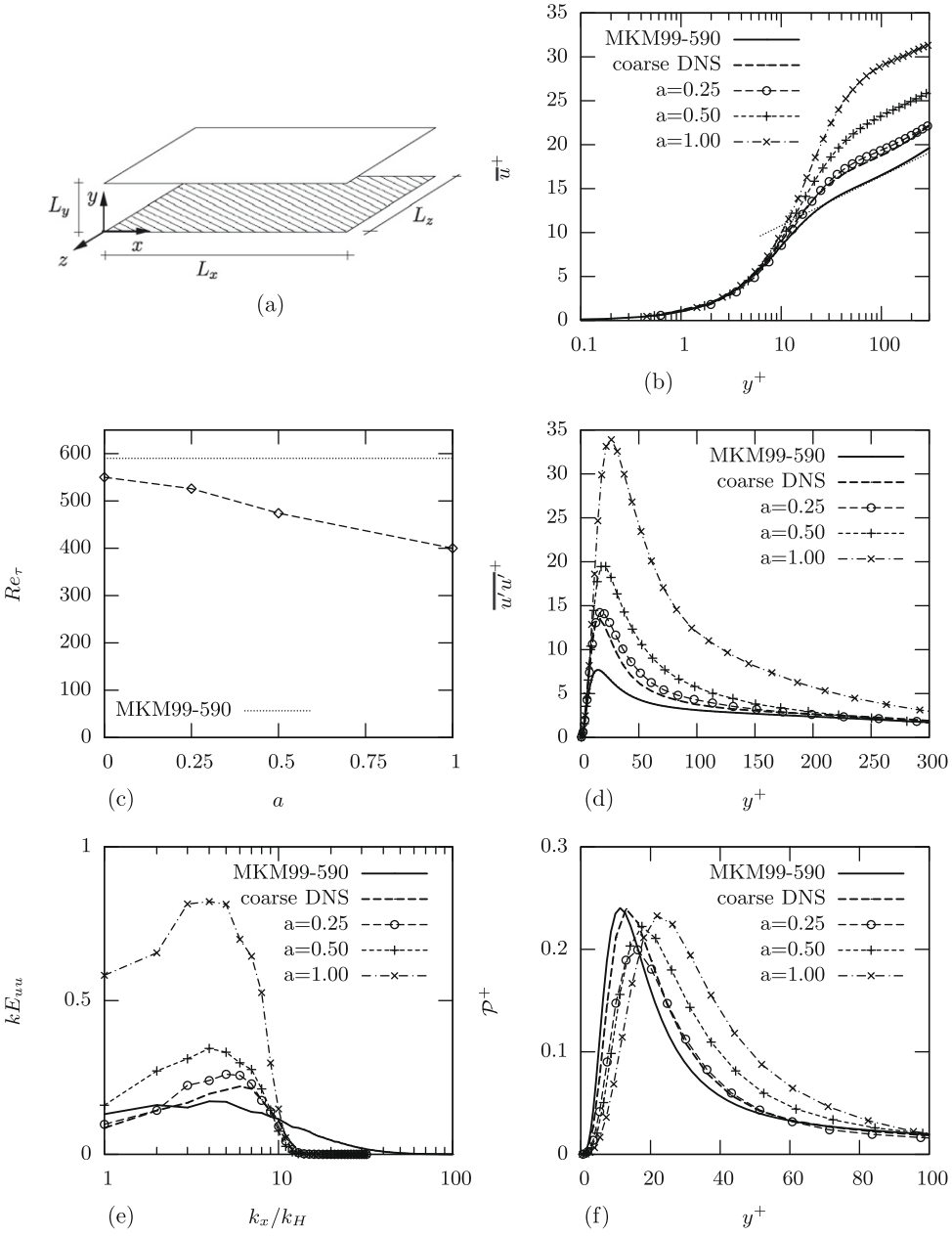

Fig. 2. The effect of varying the filter size a for plane channel flow. (a) Definition sketch; (b) average velocity; (c) shear-Reynolds number, Re_τ; (d) streamwise variance, $\overline{u'u'}$; (e) streamwise spectrum E_{uu} in midplane; (f) production of turbulent kinetic energy.

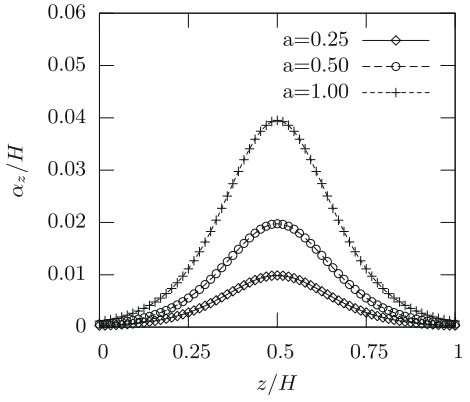

Fig. 3. The distribution of α as a function of y.

respectively. The simulation with $a = 0.25$ has little influence on the average velocity, but as a increases the profiles deviate more and more from their desired value. The source of these deviations is a decreasing wall-shear stress. Shown in Fig. 2c is the shear-Reynolds number $\mathrm{Re}_\tau = u_\tau\delta/\nu$ as a function of a. The dashed line corresponds to the expected value ($\mathrm{Re}_\tau = 590$). The coarse DNS results ($a = 0$) show that the insufficient resolution results in a 10% underestimation of Re_τ. The subfilter scale model would ideally compensate this effect. However, as a is increased, Re_τ decreases up to an underestimation of 30% at $a = 1.00$.

The variance profile of the streamwise velocity component, $\overline{u'u'}$, is shown in Fig. 2d, nondimensionalized by u_τ^2. The coarse DNS overpredicts the peak of $\overline{u'u'}^+$ by a factor two, and increasing a only makes the situation worse, with a factor five overprediction at $a = 1.00$. It should be noted that part of this increase is due to the normalisation: the decrease in the friction velocity causes

$\overline{u'u'}^+$ to become larger. However, even without scaling, the variance increases a factor 2.5 when comparing the resolved DNS results to the Leray-α simulation at $a = 1$.

The peak in $\overline{u'u'}^+$ can be seen to shift outwards, indicating a thickening of the viscous wall region. The probable mechanism for a thickening of the viscous wall region resides in the modification of the momentum-flux $\overline{\widetilde{v}'u'}$ in the buffer layer. The filtering of v will damp near-wall fluctuations, thereby reducing the turbulent momentum flux. As a result, the turbulence transport takes over further away from the wall than without filtering.

To get an idea of the typical lengthscales that cause the overprediction in the variance, the spatial spectrum of $\overline{u'u'}$ is presented. The spectrum is obtained by one-dimensional Fast Fourier Transforms (FFT) in the streamwise (spanwise) direction, and averaging over the other homogeneous direction. In addition, the spectrum is averaged over about 60 typical timescales to eliminate slow transients. In Fig. 2e, the spectrum of the streamwise velocity u is shown in the midplane of the channel. The coarse DNS slightly underpredicts the variance on the large scales and overpredicts the variance at the intermediate wavenumbers. When a is increased, first the variance increases at intermediate wavenumbers. For larger a, a significant increase in the variance occurs for the large wavenumbers as well. It should be noted that in the midplane, the difference between the DNS and the Leray-α model is relatively small; in the viscous wall region, the difference would be even greater.

More insight into the enhanced variances may be obtained by studying the budget for turbulent kinetic energy (TKE). The equation of TKE can be obtained by multiplying the fluctuating part of (1) by u_i' and averaging over the homogeneous directions and over time. The average $\bar{\cdot}$ is denoted by an overline. This results in

$$0 = \underbrace{-\overline{\widetilde{v}'u'}\partial_y\overline{u}}_{\mathscr{P}} \underbrace{-\nu\overline{(\partial_j u_i')(\partial_j u_i')}}_{\varepsilon} \underbrace{-\partial_y(\overline{\widetilde{v}'e'} - \nu\partial_y e + \overline{v'p'})}_{\mathscr{T}}, \tag{14}$$

where $e = \frac{1}{2}\overline{u_i'u_i'}$ and $e' = \frac{1}{2}u_i'u_i'$; $\mathscr{P}$, ε and $\mathscr{T}$ represent production, dissipation and transport of turbulent kinetic energy, respectively. The smoothed transport velocity directly modifies the shear production term $\mathscr{P}$ and the transport of the velocity fluctuations $\overline{\widetilde{v}'e'}$.

The production of TKE is shown in Fig. 2f, nondimensionalized by u_τ^4/ν. The thickening of the viscous wall region is clear in the profile of $\mathscr{P}^+$, where the peak (which occurs where the viscous stress is equal to the Reynolds stress) shifts from about $y^+ = 15$ for the coarse DNS to around $y^+ = 30$ for $a = 1.00$. Note also that the width of the production peak increases: only at $y^+ = 80$ is $\mathscr{P}$ at the value of the reference DNS for $a = 1.00$.

The fact that the variance increases while the production of TKE remains roughly the same is one of the intriguing features of the Leray-α model. Because of the attenuation of small-scale dynamics (Fig. 1), it is to be expected that the total variance will increase due to a slowing down of the cascade at high wavenumbers. A recent study (Graham et al., 2007) suggests that the variance accumulation at subfilter scales is even higher; for the LANS-α model, the small scales seem to behave as "rigid rotators" which are advected passively by the larger scales.

4.2. Rayleigh–Bénard convection

Rayleigh–Bénard convection (RB) is generated when a fluid in between two flat plates is heated from the bottom and cooled from the top (Fig. 4a). The system can be characterized by the Prandtl number $\mathrm{Pr} = \nu\kappa^{-1}$ and the Rayleigh number $\mathrm{Ra} = \beta g\Delta\Theta H^3(\nu\kappa)^{-1}$. The system reacts by a convective motion which is characterized by the Reynolds number $\mathrm{Re} = UH\nu^{-1}$ and by an enhanced heat transfer through the Nusselt number $\mathrm{Nu} = \phi H(\kappa\Delta\Theta)^{-1}$. Here U is a characteristic velocity and ϕ the realised heat-flux at the wall. Both Re and Nu are non-trivial functions of Ra and Pr and are still the subject of ongoing research (e.g. Ahlers et al., 2009). The coordinate system is defined with the z-direction pointing upwards and the gravity vector is in the negative z-direction.

The medium has most material properties of water except for the Prandtl number, which is taken as $\mathrm{Pr} = 1$ instead of 7 to relax the computational demands (van Reeuwijk et al., 2008); the viscosity $\nu = 1.07 \times 10^{-6}\ \mathrm{m^2/s}$, expansion coefficient $\beta = 1.74 \times 10^{-4}\ K^{-1}$, $\Delta\Theta = 2\ \mathrm{K}$, with $T_0 = \Delta\Theta/2$ and $T_1 = -\Delta\Theta/2$. The domain size $L_x \times L_y \times L_z$ is $\Gamma H \times \Gamma H \times H$, with $H = 0.15$ m and the aspect ratio $\Gamma = 4$. Fixed temperature and no-slip velocity boundary conditions are enforced at the top and bottom plates. Periodic boundary conditions are used for the sidewalls.

The simulation of a buoyancy driven flow requires the extension of the Leray-α model with a transport equation for temperature. This raises the question whether the advection of scalars should be with the filtered or the unfiltered velocity. Here the same modified advection operator will be used for all transported quantities, i.e. advective transport with $\widetilde{u}_i$. Invoking the Boussinesq approximation, the effect of buoyancy can be included by introducing a body force $\beta g_i\Theta$ in the momentum equations only. After the extension with a transport equation of temperature and with the additional body force, the Leray-α model becomes

$$\partial_t u_i + \widetilde{u}_j\partial_j u_i = \nu\partial_j^2 u_i - \partial_i p - \beta g_i\Theta, \tag{15}$$

$$\partial_t\Theta + \widetilde{u}_j\partial_j\Theta = \nu\partial_j^2\Theta. \tag{16}$$

In the current coordinate system, the gravity is in the negative z-direction as $g_i = -g\delta_{i3}$. Due to the homogeneity and the absence of a forcing in the x and y direction, $\overline{u}_i = 0$, and the system is statistically one-dimensional. One of the characteristic features of RB is that the total vertical heat-flux through the fluid is constant. Averaging over the homogeneous directions, integrating (16) with respect to z and substituting the Dirichlet boundary conditions for temperature results in

$$\overline{\widetilde{w}'\Theta'} - \kappa\partial_z\overline{\Theta} = \frac{\kappa\Delta\Theta}{H}\mathrm{Nu}. \tag{17}$$

Note that the turbulent heat-flux is in terms of the filtered velocity $\widetilde{u}_i$. However, the TKE production by buoyancy is given by $\overline{w'\Theta'}$ (18) and this mismatch will prove to be of importance, as discussed below.

Although many results can be found in the literature on direct simulation of Rayleigh–Bénard convection in wide aspect ratios (Domaradzki et al., 1994; Kerr, 1996), no database is available as for plane channel flow and side-heated convection simulations. Therefore, the results will be compared to our own DNS results (van Reeuwijk et al., 2005; van Reeuwijk et al., 2008) at $\mathrm{Ra} = 10^7$ and $\mathrm{Pr} = 1$. The grid for the DNS is $256 \times 256 \times 256$ cells which is of sufficient resolution not to require grid clustering near the wall. The grid resolution for the Leray-α and coarse DNS simulations is $80 \times 80 \times 64$, which is again chosen such that it is too coarse for DNS but is not yet dominated by numerical contamination. Here, grid clustering is applied such that of the 64 wall-normal points, 8 are present in each thermal boundary layer.[1]

One of the most important integral flow properties in RB is the Nusselt number, Nu. At the current Ra and Pr, the DNS gives that $\mathrm{Nu} = 16.1$. The coarse DNS significantly overpredicts this value with $\mathrm{Nu} = 20$ (Fig. 4b), due to the insufficient resolution. The influ-

[1] Because most transport occurs perpendicular to the wall, the hydrodynamic and thermal boundary layers are commonly defined as the region from the wall to where the kinetic energy and temperature variance peaks, respectively.

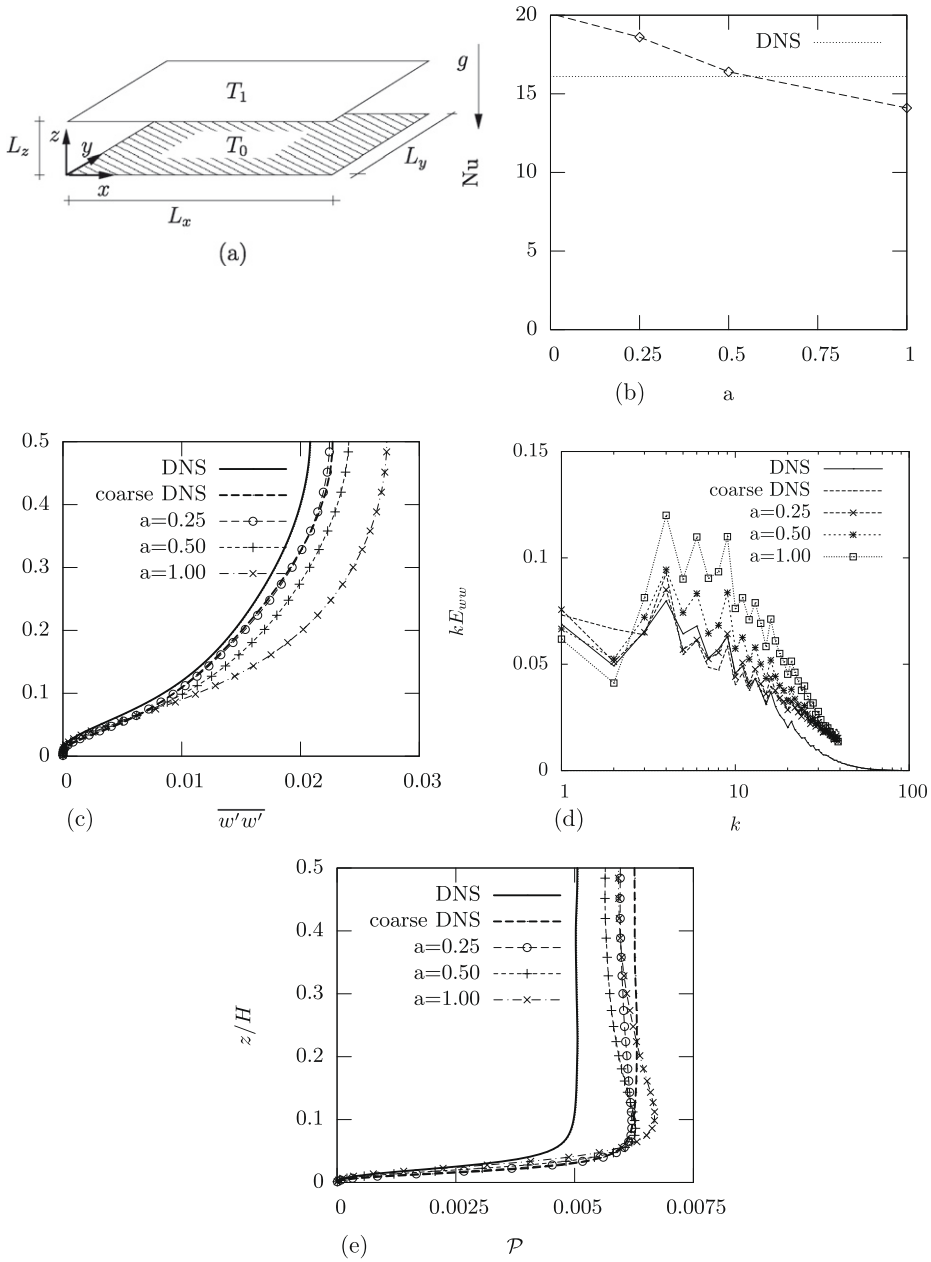

Fig. 4. The effect of varying the filter size a for Rayleigh–Bénard convection. (a) Definition sketch; (b) Nusselt number, Nu; (c) wall-normal variance, $\overline{w'w'}$; (d) wall-normal spectrum E_{ww} in midplane; (e) production of turbulent kinetic energy.

ence of the Leray-α model is to decrease Nu, and at $a = 0.50$ the Nusselt number Nu is approximately at its expected value.

In Fig. 4c, the wall-normal velocity variance $\overline{w'w'}$ is shown, normalized by U^2 where $U = \sqrt{\beta g \Delta \Theta H}$ is the free-fall velocity. As for the plane channel flow, the variance can be seen to increase as a becomes larger. Spatial spectra are collected by performing a 2D FFT and integrating over circles $k_x^2 + k_y^2 = k^2$. Shown in Fig. 4d is the spectrum of the vertical velocity in the midplane. The increase of variance for the coarse DNS seems to be mainly concentrated at the large scales (low wavenumbers). When a is increased, it can be seen that the variance at the intermediate wavenumbers increases.

As before, we study the equation of TKE, which is for Rayleigh–Bénard convection given by

$$0 = \underbrace{\beta g \overline{w'\Theta'}}_{\mathscr{P}} - \underbrace{\nu \overline{(\partial_j u_i')(\partial_j u_i')}}_{\varepsilon} - \underbrace{\partial_z (\overline{\widetilde{w}'e'} - \nu \partial_z e + \overline{w'p'})}_{\mathscr{T}}. \tag{18}$$

For this flow case, there is no production on average of turbulent kinetic energy by shear and the only effect of the filtering is in a modified transport of the velocity fluctuations $\overline{\widetilde{w}'e'}$.

The production term $\mathscr{P}$ is shown in Fig. 4e, nondimensionalized by $(\beta g \Delta \Theta H)^{3/2}/H$. The coarse DNS overestimates $\mathscr{P}$, which is consistent with the overestimation of Nu as these are directly coupled for RB by the exact relation (see e.g. Siggia, 1994; Grossmann and Lohse, 2000) $\langle \mathscr{P} \rangle_z = \langle \varepsilon \rangle_z = \frac{\nu^3}{H^4} \mathrm{Ra}(\mathrm{Nu} - 1)\mathrm{Pr}^{-2}$. The total production decreases for $a = 0.25$ and $a = 0.50$, but for $a = 1.00$, $\mathscr{P}$ increases again. This is not consistent with the monotonically decreasing trend for Nu (Fig. 4b). Furthermore, the shape of the production profile changes: the constant production in the bulk is replaced by a production profile which peaks near the hydrodynamic boundary layers. Both the trendbreak and the change of shape are the results of a disparity between the buoyancy production

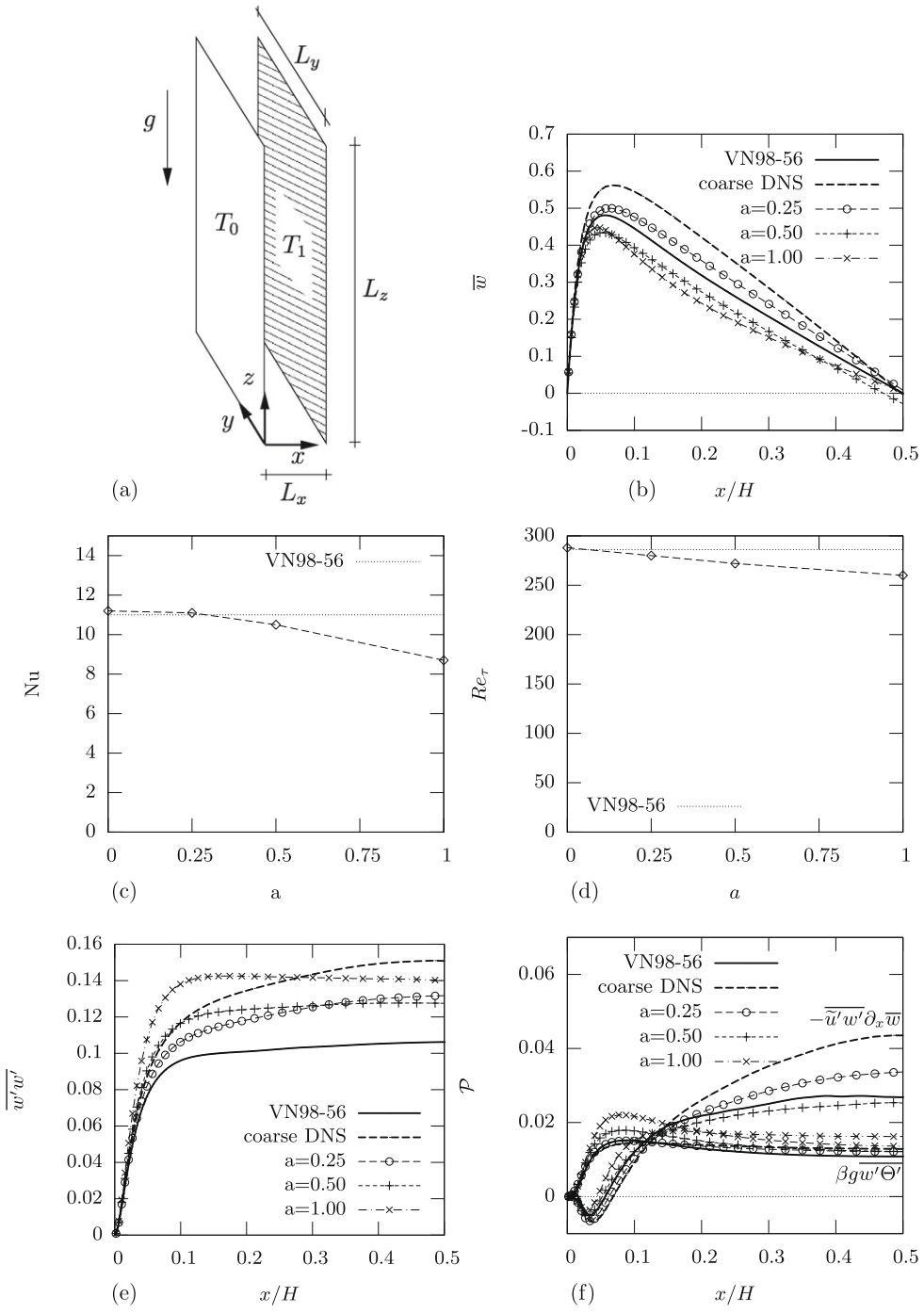

Fig. 5. The effect of varying the filter size a for side-heated convection. (a) Definition sketch; (b) average velocity; (c) Nusselt number, Nu; (d) shear-Reynolds number, Re_τ; (e) streamwise variance, $\overline{w'w'}$; (f) production of turbulent kinetic energy.

term $\mathscr{P} = \beta g\overline{w'\Theta'}$ and the turbulent heat-flux $\overline{\widetilde{w}'\Theta'}$. This is a fundamental issue which will be discussed in detail in Section 5.

4.3. Side-heated vertical channel

The side-heated vertical channel is a case where both buoyancy and shear production are important. The flow has several unusual features, such as negative shear production in the boundary layers[2] and counter-gradient heat fluxes. The side-heated vertical channel has been studied intensively both experimentally (Betts and Bokhari, 2000) and by direct simulation (Boudjemadi et al., 1997; Versteegh, 1998; Versteegh and Nieuwstadt, 1998, 1999). The flow geometry for the side-heated vertical channel is sketched in Fig. 5a. For this case, the x-direction in the wall-normal direction and the z-direction is pointing upward. The Leray-α simulations will be compared to the DNS database of Versteegh and Nieuwstadt (1999). The size of the domain is $L_x \times L_y \times L_z = H \times 6H \times 12H$. The unusually large domain size is required to prevent long-range correlations from influencing the statistics (Versteegh and Nieuwstadt, 1998). The medium is air with a viscosity $\nu = 1.0 \times 10^{-5}\ \mathrm{m^2/s}$, expansion coefficient

[2] The hydrodynamic boundary layer thickness can be determined using the maximum of $\bar{w}$, and the thermal boundary layer thickness by the maximum of the temperature variance.

$\beta = 3.3 \times 10^{-3}$ K^{-1} and a Prandtl number Pr = 0.709. The distance H between the plates is $H = 0.2$ m and with a temperature difference $\Delta\Theta = 2.7$ K with $T_0 = \Delta\Theta/2$ and $T_1 = -\Delta\Theta/2$. The Rayleigh number $\mathrm{Ra} = \beta g \Delta\Theta H^3 (\nu\kappa)^{-1}$ for this case is $\mathrm{Ra} = 5 \times 10^6$. The resolution for the coarse DNS is $64 \times 96 \times 192$, which as before is chosen such that the grid is too coarse for accurate predictions but fine enough to prevent that the results are dominated by numerical contamination. The statistics have been collected over 25 typical turnover times.

In accordance with Versteegh and Nieuwstadt (1998), and Versteegh (1998), a body force is introduced which ensures a zero mass-flux. The advantage is that this suppresses slow transients, thereby reducing the required simulation time. In addition, omitting the body force results in a nonzero mass flux at high a, which obfuscates comparison with other simulations.

The average velocity profile is shown in Fig. 5b, normalized by the free-fall velocity $\sqrt{\beta g \Delta\Theta H}$. The coarse DNS overestimates the average flow velocity in the channel. When increasing a, the velocity decreases and the flow profile is approximately correctly predicted for $a = 0.25$. For $a = 0.50$, the velocity is underpredicted. At $a = 1.00$, the velocity profile remains at roughly the same amplitude as for $a = 0.5$ but here a 'kink' can be observed in the mean velocity around $x/H = 0.2$, which is not present in the other simulations. This kink is responsible for the shift of the shear production term $\widetilde{\overline{u}'w'}\partial_x\bar{w}$ from the center to the near-wall region.

The results for $\mathrm{Nu} = \partial_x\overline{\Theta}|_w H/\kappa\Delta\Theta$ as a function of a are shown in Fig. 5c. The increase in the average velocity does not influence Nu very much for the coarse DNS. The trend for increasing a is that Nu decreases, similar to Rayleigh–Bénard convection. Around $a = 0.25$, Nu is at its expected value, and above this value, Nu is underpredicted. The shear-Reynolds number Re_τ is defined as $\mathrm{Re}_\tau = u_\tau H/\nu$. The influence of a is relatively small for this flowcase (Fig. 5d), with an underprediction of Re_τ of 10% at $a = 1.00$.

The streamwise velocity variance profile $\overline{w'w'}$ is shown in Fig. 5e, nondimensionalized by $\beta g \Delta\Theta H$. The coarse DNS overestimates the variance by 50% in the bulk. Here the effect of increasing a is to decrease the variance for $a = 0.25$. As a is increased further, the variance becomes practically constant in the bulk ($a = 0.50$), after which the maximum shifts from the center to the near-wall region ($a = 1.00$).

The equation of TKE for the side-heated vertical channel is given by

$$0 = \underbrace{\beta g \overline{w'\Theta'} - \widetilde{\overline{u}'w'}\partial_x\bar{w}}_{\mathscr{P}} - \underbrace{\nu\overline{(\partial_j u_i')(\partial_j u_i')}}_{\varepsilon} - \underbrace{\partial_x(\widetilde{\overline{u}'e'} - \nu\partial_x e + \overline{u'p'})}_{\mathscr{T}}. \tag{19}$$

For this flow case, there is production of TKE both by shear and by buoyancy. Both components of $\mathscr{P}$ are shown as a function of z/H in Fig. 5f. Here, it can be seen that the lack of resolution mainly affects the shear production term $-\widetilde{\overline{u}'w'}\partial_x\bar{w}$ through the overestimation of the average velocity (Fig. 5b). The effect of increasing a reduces the shear production and the production is estimated appropriately at $a = 0.50$. At $a = 1.00$, the buoyancy production term changes little with respect to $a = 0.50$, but the shear production term changes dramatically.

5. Discussion

The simulations show two major trends. First, gradients at the wall (as reflected in integral quantities like Re_τ and Nu) tend to decrease. Both for Rayleigh–Bénard convection and the side-heated vertical channel, coarse DNS overpredicts wall gradients, and the Leray-α model can improve results. In the case that coarse DNS underpredicts gradients at the wall, as for the plane channel flow, the Leray-α model does not improve the results.

Second, the variances tend to increase as a function of α, specifically at the low and intermediate wavenumbers. In view of the model spectrum (Fig. 1), which predicts an increase in the variance at wavenumbers larger than k_α only, this may be quite surprising. However, this seems to be an intrinsic property of the Leray-α model. Simulations with the Leray-α model in absence of walls (Geurts and Holm, 2006; Graham et al., 2008) also results in enhanced variances and the low and intermediate wave lengths. The presence of a wall seems to enhance this property of the model, due to an increase in the turbulent shear production term.

In simulations with coarse grids, a significant part of the fluctuations are sub-grid, and separate modeling may be required (e.g. Carati et al., 2001). Therefore, a pragmatic solution to remedy the increased variances may be to add some extra diffusion to the model. This may be done in several ways: (1) by using a simple eddy-viscosity model; (2) by using a dynamic Smagorinsky procedure; and (3) by using a spectral dissipation procedure. It is clear that this procedure would have to be done with care, as one could easily overwhelm the Leray-α contribution to the subfilter stress. The tensor-diffusivity model (also called Clark model) (Winckelmans et al., 2001), is a good example of a model which significantly benefits from some additional dissipation. This filter reproduces approximately 90% of the subfilter stresses in *a priori* studies. However, in *a posteriori* studies, the tensor diffusivity model requires additional dissipation (Winckelmans et al., 2001). Extra dissipation may be unavoidable in particular when using Leray-α with relatively coarse meshes. In this study, the resolution was chosen such that coarse DNS simulations were incapable of reproducing correct statistics but were not dominated by wiggles. When even coarser grids would have been used, the absence of additional dissipation leads to a deterioration of the results of the Leray-α model.

In this study we chose to keep the filter as close as possible to the original formulation (Cheskidov et al., 2005). The filtering requires inverting a Helmholtz equation for all three velocity components, which is computationally expensive. In addition, the projection step to make $\widetilde{u}_i$ divergence-free requires solving another Poisson equation. Even though the computational overhead for solving a Poisson equation is minimized by using FFTs in the homogeneous directions, this procedure is more expensive than conventional SGS models. To reduce the number of operations, one could use explicit filters (Geurts and Holm, 2006; Liu et al., 2008) or apply (4) but with only one or two Jacobi iterations (Verstappen, 2008).

An important question for future research is related to the influence of the filter type. It is not inconceivable that an explicit filter (i.e. a filter that does not require solving a Poisson equation, such as a top-hat filter) might perform better than the Helmholtz filter. Indeed, the Helmholtz filter suffers from $\mathscr{L}(0) \neq 0$ even for uniform α, which violates the filtering framework (van Reeuwijk et al., 2006). A projection method was required to remedy this problem. In addition, the Helmholtz filter does not have compact support, causing the filtered velocity to be influenced relatively strongly by large fluctuations far away.

The inclusion of the buoyancy term in the Leray-α model has to be done with care. In the direct simulations of Rayleigh–Bénard convection, the average buoyancy production $\mathscr{P} = \beta g \overline{w'\Theta'}$ is constant in the bulk, as $\mathscr{P}$ depends directly on the turbulent heat flux $\overline{w'\Theta'}$ (which is constant in the bulk). This is not the case for the Leray-α model, where a peak in $\mathscr{P}$ is created near the hydrodynamic boundary layer (Fig. 4e). This change is a direct consequence of the modification of the turbulent heat flux. In the present formulation (15) and (16), the direct coupling between TKE production and heat-flux is broken, as the equations for TKE and average heat-flux are given by (see also Appendix A):

$$\partial_z\left(\widetilde{\overline{w}'e'} + \overline{p'w'} - \nu\partial_z e\right) = \beta g \overline{w'\Theta'} - \varepsilon, \tag{20}$$

$$\widetilde{\overline{w}'\Theta'} - \kappa\partial_z\overline{\Theta} = \frac{\kappa\Delta\Theta}{H}\mathrm{Nu}. \tag{21}$$

The buoyancy production term is given by $\beta g\overline{w'\Theta'}$, while the turbulent heat flux (which is constant in the bulk) is given by $\overline{\widetilde{w}'\Theta'}$ (17). The difference between $\overline{w'\Theta'}$ and $\overline{\widetilde{w}'\Theta'}$ can be calculated by substituting $w = \widetilde{w} - \partial_j\alpha_j^2\partial_j\widetilde{w}$ into $\overline{w'\Theta'}$, which results in

$$\overline{w'\Theta'} = \overline{\widetilde{w}'\Theta'} - \partial_z(\alpha_z^2\overline{\Theta'\partial_z\widetilde{w}'}) + \alpha_j^2\overline{(\partial_j\Theta')(\partial_j\widetilde{w}')}. \tag{22}$$

Interestingly, the two extra terms on the right-hand side correspond to terms typically encountered in the transport equation of $\overline{w'\Theta'}$ (Hanjalić, 2002). The first is normally associated with the molecular diffusive transport, and the second with the dissipative cross-correlation term, although the sign is opposite here.

For buoyancy driven flows, the variation of α as a function of the wall-normal coordinate z seems be of importance for the variation of $\mathscr{P}$ over the vertical in the bulk. Indeed, the preliminary simulations with constant α (and free-slip conditions for $\widetilde{u}$) did not have a variation of $\mathscr{P}$ over the height (van Reeuwijk et al., 2007). At $a = 0.5$, the difference of $\mathscr{P}$ between the peak value at the edge of the boundary layer and the core is 10% (Fig. 4e). This is quite a large difference, and it seems worthwhile to explore whether this effect can be circumvented. The first and most obvious way is to experiment with different filters. Another option is to modify the temperature equation. Instead of holding on to the same advection operator for all transported quantities, one could apply the modified advection operator $\widetilde{u}_j\partial_j$ to the momentum equations only. For the other transported quantities, $u_j\partial_j$ could be used, with the understanding that u_j is also a regularized velocity. This would directly restore the coupling between the turbulent heat-flux and the buoyancy production. However, the danger in a formulation like this may be an excess of variance at small scales, which results in a high-wavenumber forcing contaminating the simulation.

6. Concluding remarks

Numerical simulations of the Leray-α model have been carried out for plane channel flow, Rayleigh–Bénard convection and the side-heated vertical channel. The simulations have been compared to DNS and coarse DNS. In general, the simulations show two trends. First, the viscous (and diffusive) wall region tends to thicken as a function of the filter width parameter a, which causes wall gradients such as the shear stress or the heat-flux to decrease. When coarse DNS overpredicts wall gradients, such as for Rayleigh–Bénard convection and (to a lesser extent) the side-heated vertical channel, the Leray-α model can improve the results. However, when the gradients are initially underestimated, such as for the plane channel, results do not improve. Here, additional wall-modeling may be needed to enhance turbulence levels in the near-wall region. Second, the variance at low and intermediate wavenumbers increases upon increasing the filter size parameter a. This leads to overpredicted variance in the velocity field which is undesired.

An important point for buoyancy driven flows is how to include a temperature forcing into the Leray-α model. Indeed, the intuitive extension (15) and (16) causes the production of TKE by buoyancy to be no longer directly coupled to the turbulent heat-flux. For Rayleigh–Bénard convection, this leads to a varying TKE production in the bulk (and as a function of a).

In this paper, the performance of the Leray-α model was assessed for three wall-bounded flows. The Leray-α model was implemented in its original form, i.e. with the Helmholtz filter. This study indicates that, within this formulation, the potential of the Leray-α model is rather limited for wall-bounded flows. Indeed, the overpredicted variances, in particular the accumulation of energy on the low and intermediate wavenumbers pose a challenge for accurate predictions with the Leray-α model. A study on alternative filter types, potentially remedying the aforementioned downsides of the Helmholtz filter, would be a valuable next step.

Acknowledgments

M.v.R. thanks Prof. Darryl Holm for an inspiring stay at Imperial College in 2005. We would like to thank Dr. Roel Verstappen and Prof. Bernard Geurts for several useful discussions. This work is part of the research programme of the Stichting voor Fundamenteel Onderzoek der Materie (FOM), which is financially supported by the Nederlandse Organisatie voor Wetenschappelijk Onderzoek (NWO). The computations were sponsored by the Stichting Nationale Computerfaciliteiten (NCF).

Appendix A. Changes in the dissipation rate for Rayleigh–Bénard convection

The relations relating the volume-averaged dissipation rate of kinetic energy $\langle\varepsilon\rangle_z$ and temperature variance $\langle\varepsilon_\Theta\rangle_z$ to the Rayleigh number Ra, the Prandtl number Pr and the Nusselt number Nu are given by (Grossmann and Lohse, 2000; Siggia, 1994)

$$\langle\varepsilon\rangle_z = \frac{\nu^3}{H^4}\mathrm{Ra}(\mathrm{Nu}-1)\mathrm{Pr}^{-2}, \tag{23}$$

$$\langle\varepsilon_\Theta\rangle_z = \kappa\frac{\Delta\Theta^2}{H^2}\mathrm{Nu}, \tag{24}$$

where $\langle\varepsilon\rangle_z$ and $\langle\varepsilon_\Theta\rangle_z = \langle\varepsilon_{\Theta,\mathrm{av}}\rangle_z + \langle\varepsilon_{\Theta,\mathrm{fl}}\rangle_z$ are defined as

$$\langle\varepsilon\rangle_z = \nu\langle\overline{(\partial_j u_i')(\partial_j u_i')}\rangle_z,$$
$$\langle\varepsilon_{\Theta,\mathrm{av}}\rangle_z = \kappa\langle(\partial_z\overline{\Theta})^2\rangle_z,$$
$$\langle\varepsilon_{\Theta,\mathrm{fl}}\rangle_z = \kappa\langle\overline{(\partial_j\Theta')(\partial_j\Theta')}\rangle_z.$$

Here, $\langle\cdot\rangle_z$ represents the averaging over the entire fluid layer, and the combination $\langle\bar{\cdot}\rangle_z$ is equal to a volume- or ensemble-average, when the system is ergodic. Below we will derive the relations for $\langle\varepsilon\rangle_z$ and $\langle\varepsilon_\Theta\rangle_z$ for the Leray-α model.

Eqs. (23) and (24) are obtained from the equations of the vertical heat-flux, turbulent kinetic energy and the two equations for temperature variance. In the case of the Leray-α model, these equations are given by

$$\overline{\widetilde{w}'\Theta'} - \kappa\partial_z\overline{\Theta} = \frac{\kappa\Delta\Theta}{H}\mathrm{Nu}, \tag{25}$$

$$\partial_z\left(\overline{\widetilde{w}'e'} + \overline{p'w'} - \nu\partial_z e\right) = \beta g\overline{w'\Theta'} - \varepsilon, \tag{26}$$

$$\partial_z\left(\overline{\widetilde{w}'\Theta'}\;\overline{\Theta} - \kappa\partial_z\frac{1}{2}\overline{\Theta}\;\overline{\Theta}\right) = \overline{\widetilde{w}'\Theta'}\partial_z\overline{\Theta} - \varepsilon_{\Theta,\mathrm{av}}, \tag{27}$$

$$-\kappa\partial_z^2\frac{1}{2}\overline{\Theta'\Theta'} = -\overline{\widetilde{w}'\Theta'}\partial_z\overline{\Theta} - \varepsilon_{\Theta,\mathrm{fl}}, \tag{28}$$

where $e' = u_i'u_i'$ and $e = \overline{u_i'u_i'}$.

Averaging these expressions over the height, we obtain

$$\langle\overline{\widetilde{w}'\Theta'}\rangle_z = \frac{\kappa\Delta\Theta}{H}(\mathrm{Nu}-1), \tag{29}$$

$$\langle\varepsilon\rangle_z = \beta g\langle\overline{w'\Theta'}\rangle_z, \tag{30}$$

$$-\kappa\frac{\Delta\Theta^2}{H^2}\mathrm{Nu} = \langle\overline{\widetilde{w}'\Theta'}\partial_z\overline{\Theta}\rangle_z - \langle\varepsilon_{\Theta,\mathrm{av}}\rangle_z, \tag{31}$$

$$0 = -\langle\overline{\widetilde{w}'\Theta'}\partial_z\overline{\Theta}\rangle_z - \langle\varepsilon_{\Theta,\mathrm{fl}}\rangle_z. \tag{32}$$

Adding (31) and (32), the exact relation for $\langle\varepsilon_\Theta\rangle_z$, (24) is obtained. However, this is not the case for the relation of the dissipation rate of TKE (23). Instead of the heat-flux based on the filtered velocity $\overline{\widetilde{w}'\Theta'}$, (23) contains the heat-flux of the unfiltered velocity as

$\overline{w'\Theta'}$. Substituting $w = \widetilde{w} - \partial_j \alpha_j^2 \partial_j \widetilde{w}$ (so not correcting for compressibility effects), the two heat-fluxes are non-trivially coupled by

$$\overline{w'\Theta'} = \overline{\widetilde{w}'\Theta'} - \partial_z \alpha_j^2 \overline{\Theta' \partial_z \widetilde{w}'} + \alpha_j^2 \overline{(\partial_j \Theta')(\partial_j \widetilde{w}')}. \tag{33}$$

Interestingly, the two extra terms on the right-hand side correspond to terms typically encountered in the transport equation for the turbulent heat-flux (Hanjalić, 2002). The first is normally associated with the molecular diffusive transport, and the second with the dissipative cross-correlation term, although the sign is opposite here. Averaging (33) over the height and substituting the result into (30) using (29), gives that $\langle \varepsilon \rangle_z$ is given by

$$\langle \varepsilon \rangle_z = \frac{\nu^3}{H^4} \mathrm{Ra}(\mathrm{Nu} - 1)\mathrm{Pr}^{-2} + \beta g \langle \alpha^2 \overline{(\partial_j \Theta')(\partial_j \widetilde{w}')} \rangle_z. \tag{34}$$

References

Ahlers, G., Grossmann, S., Lohse, D., 2009. Heat transfer and large scale dynamics in turbulent Rayleigh–Bénard convection. Rev. Mod. Phys. 81, 503–537.

Betts, P.L., Bokhari, I.H., 2000. Experiments on turbulent natural convection in an enclosed tall cavity. Int. J. Heat Fluid Flow 21 (6), 675–683.

Boudjemadi, R., Maupu, V., Laurence, D., LeQuere, P., 1997. Budgets of turbulent stresses and fluxes in a vertical slot natural convection flow at Rayleigh Ra = 10(5) and 5.4 10(5). Int. J. Heat Fluid Flow 18 (1), 70–79.

Carati, D., Winckelmans, G.S., Jeanmart, H., 2001. On the modelling of the subgrid-scale and filtered-scale stress tensors in large-eddy simulation. J. Fluid Mech. 441 (August), 119–138.

Chen, S., Foias, C., Holm, D.D., Olson, E., Titi, E.S., Wynne, S., 1999a. The Camassa–Holm equations and turbulence. Physica D 133, 49–65.

Chen, S., Foias, C., Holm, D.D., Olson, E., Titi, E.S., Wynne, S., 1999b. A connection between the Camassa–Holm equations and turbulent flows in channels and pipes. Phys. Fluids 11 (8), 2343–2353.

Chen, S., Holm, D.D., Margolin, L.G., Zhang, R., 1999c. Direct numerical simulations of the Navier–Stokes alpha model. Physica D 133, 66–83.

Cheskidov, A., Holm, D.D., Olson, E., Titi, E.S., 2005. On a Leray-alpha model of turbulence. Proc. Roy. Soc. Lond. A – Mater. 461 (2055), 629–649.

Clark, R.A., Ferziger, J.H., Reynolds, W.C., 1979. Evaluation of sub-grid-scale models using an accurately simulated turbulent-flow. J. Fluid Mech. 91 (March), 1–16.

Domaradzki, J.A., Liu, W., Hartel, C., Kleiser, L., 1994. Energy-transfer in numerically simulated wall-bounded turbulent flows. Phys. Fluids 6 (4), 1583–1599.

Ferziger, J.H., Perić, M., 2002. Computational Methods for Fluid Dynamics. Springer.

Foias, C., Holm, D., Titi, E., 2001. The Navier–Stokes-alpha model of fluid turbulence. Physica D, 505–519.

Geurts, B.J., Holm, D.D., 2006. Leray and LANS-alpha modelling of turbulent mixing. J. Turbul. 7 (10), 1–33.

Graham, J.P., Holm, D.D., Mininni, P.D., Pouquet, A., 2007. Highly turbulent solutions of the Lagrangian-averaged Navier–Stokes alpha model and their large-eddy-simulation potential. Phys. Rev. E 76 (5), 056310.

Graham, J.P., Holm, D.D., Mininni, P.D., Pouquet, A., 2008. Three regularization models of the Navier–Stokes equations. Phys. Fluids 20 (3), 035107.

Grossmann, S., Lohse, D., 2000. Scaling in thermal convection: a unifying theory. J. Fluid Mech. 407, 27–56.

Hanjalić, K., 2002. One-point closure models for buoyancy-driven turbulent flows. Ann. Rev. Fluid Mech. 34, 321–347.

Holm, D.D., 1999. Fluctuation effects on 3D Lagrangian mean and Eulerian mean fluid motion. Physica D 133 (1–4), 215–269.

Holm, D.D., 2002. Variational principles for Lagrangian-averaged fluid dynamics. J. Phys. A – Math. Gen. 35, 679–688.

Holm, D.D., Marsden, J.E., Ratiu, T.T., 1998. Euler–Poincaré models of ideal fluids with nonlinear dispersion. Phys. Rev. Lett. 80 (19), 4173–4176.

Kerr, R.M., 1996. Rayleigh number scaling in numerical convection. J. Fluid Mech. 310, 139–179.

Leonard, A., 1974. Energy cascade in large-eddy simulations of turbulent fluid flows. Adv. Geophys. 18 (3), 237.

Leray, J., 1934. Essai sur le mouvement d'un fluide visqueux emplissant l'espace. Acta Math. 63, 193–248.

Liu, Y., Tucker, P.G., Kerr, R.M., 2008. Linear and nonlinear model large-eddy simulations of a plane jet. Comput. Fluids 37, 439–449.

Marsden, J.E., Shkoller, S., 2003. The anisotropic Lagrangian averaged Euler and Navier–Stokes equations. Arch. Ration. Mech. Anal. 166 (1), 27–46.

Mohseni, K., Kosovic, B., Shkoller, S., Marsden, J.E., 2003. Numerical simulations of the Lagrangian averaged Navier–Stokes equations for homogeneous isotropic turbulence. Phys. Fluids 15 (2), 524–544.

Moser, R.D., Kim, J., Mansour, N.N., 1999. Direct numerical simulation of turbulent channel flow up to Re-tau = 590. Phys. Fluids 11 (4), 943–945.

Pope, S.B., 2000. Turbulent Flows. Cambridge University Press.

Siggia, E.D., 1994. High Rayleigh number convection. Ann. Rev. Fluid Mech. 26, 136–168.

van Reeuwijk, M., 2007. Direct simulation and regularization modeling of turbulent thermal convection. Ph.D. Thesis, Delft University of Technology.

van Reeuwijk, M., Jonker, H.J.J., Hanjalić, K., 2005. Identification of the wind in Rayleigh–Bénard convection. Phys. Fluids 17 (5), 051704.

van Reeuwijk, M., Jonker, H.J.J., Hanjalić, K., 2006. Incompressibility of the Leray-α model for wall-bounded flows. Phys. Fluids 18, 018103.

van Reeuwijk, M., Jonker, H.J.J., Hanjalić, K., 2007. Applying the Leray-α model to unbounded Rayleigh–Bénard convection. In: Oberlack, M., Guenther, S., Weller, T., Khujadze, G., Osman, A., Frewer, M., Peinke, J. (Eds.), Progress in Turbulence 2. Springer Proceedings in Physics, vol. 109. Springer.

van Reeuwijk, M., Jonker, H.J.J., Hanjalić, K., 2008. Wind and boundary layers in Rayleigh–Bénard convection. I. Analysis and modelling. Phys. Rev. E 77, 036311.

Verstappen, R., 2008. On restraining the production of small scales of motion in a turbulent channel flow. Comput. Fluids 37 (7), 887–897.

Verstappen, R.W.C.P., Veldman, A.E.P., 2003. Symmetry-preserving discretization of turbulent flow. J. Comput. Phys. 187 (1), 343–368.

Versteegh, T.A.M., 1998. Numerical simulation of turbulent natural convection between two infinite, differentially heated vertical plates. Ph.D. Thesis, Delft University of Technology.

Versteegh, T.A.M., Nieuwstadt, F.T.M., 1998. Turbulent budgets of natural convection in an infinite differentially heated vertical channel. Int. J. Heat Fluid Flow 19 (2), 135–149.

Versteegh, T.A.M., Nieuwstadt, F.T.M., 1999. A direct numerical simulation of natural convection between two infinite vertical differentially heated walls scaling laws and wall functions. Int. J. Heat Mass Transfer 42 (19), 3673–3693.

Winckelmans, G.S., Wray, A.A., Vasilyev, O.V., Jeanmart, H., 2001. Explicit-filtering large-eddy simulation using the tensor-diffusivity model supplemented by a dynamic Smagorinsky term. Phys. Fluids 13 (5), 1385–1403.